

# Beyond Single Stage Encoder-Decoder Networks: Deep Decoders for Semantic Image Segmentation

Gabriel L. Oliveira · Senthil Yogamani · Wolfram Burgard · Thomas Brox

**Abstract** Single encoder-decoder methodologies for semantic segmentation are reaching their peak in terms of segmentation quality and efficiency per number of layers. To address these limitations, we propose a new architecture based on a decoder which uses a set of shallow networks for capturing more information content. The new decoder has a new topology of skip connections, namely backward and stacked residual connections. In order to further improve the architecture we introduce a weight function which aims to re-balance classes to increase the attention of the networks to under-represented objects. We carried out an extensive set of experiments that yielded state-of-the-art results for the CamVid, Gatech and Freiburg Forest datasets. Moreover, to further prove the effectiveness of our decoder, we conducted a set of experiments studying the impact of our decoder to state-of-the-art segmentation techniques. Additionally, we present a set of experiments augmenting semantic segmentation with optical flow information, showing that motion clues can boost pure image based semantic segmentation approaches.

**Keywords** Deep Learning · Semantic Segmentation · Deep Decoder · DPDB-Block · Dynamic Weight Function · Efficient Segmentation

## 1 Introduction

Deep learning approaches have become the standard for multiple perception tasks, like classification (Simonyan et al. 2015; He et al. 2015; Huang et al. 2017), object detection

(Girshick 2015), optical flow (Ilg et al. 2017), and semantic segmentation (Long et al. 2015; Ronneberger et al. 2015; L. Chen et al. 2015; Islam et al. 2017). For dense prediction tasks, architectures that are build on Fully Convolutional Networks (FCNs) (Long et al. 2015) have become the standard approach. These networks extend classification architectures, which consist solely of a convolutional encoder and some fully connected layers, to dense prediction by replacing the fully connected layers by a convolutional decoder that recovers the resolution lost by the down-sampling operation in the encoder. While largely used and efficient in their early adoption, single encoder-decoder networks are reaching a saturation in terms of segmentation quality and efficiency per number of layers. The main bottleneck of single stage decoders is that they cannot feed-back encoder layers with context information (decoder layers), such connection can make the architecture to extract more informative features. For example, when labeling a person image region, once the feature learning areas are aware that the region contains a person, the network may focus on the person-like visual patterns.

In this paper, we aim to extend the decoder concept by proposing a new topology called Deep Decoder (DD). Deep decoders are decoder modules that not only upsample the features to a desired resolution, but also incorporate a feature learning capability to decoders by stacking multiple shallow decoder-encoder modules and connecting them in a way the shallow decoders are aware of the context information. We introduce new skip connection topologies and show that these improve the information flow, thus leading to better segmentation outputs while being computationally efficient. Deep supervision is beneficial to train deeper architectures (L. Wang et al. 2015). In our setting, it is composed of a set of outputs in each decoder. With this multi-loss approach, we update the network in a hierarchical way, which improves the gradient propagation.

---

Gabriel L. Oliveira · Wolfram Burgard · Thomas Brox  
 University of Freiburg  
 E-mail: {oliveira,burgard,brox}@cs.uni-freiburg.de  
 Senthil Yogamani  
 Valeo Inc.  
 E-mail: senthil.yogamani@valeo.com

The decoder (Deep Decoder) is the major new contribution of this work. It is further combined with the architecture block called Dual Path Dense Block (DPDB). DPDB blocks are designed to incorporate feature re-usage and new feature exploration capabilities into a single parameter efficient block. We presented the DPDB block in a preliminary conference version (Oliveira et al. 2018). A modified version, which is more focused on performance, is the main building block of the proposed encoder modules in this work.

We also introduce a class balance weight function, which improves the network’s attention to under-represented classes. The experimental evaluation shows that all the proposed measures lead to an approach that achieves state-of-the-art results on public datasets relevant for robotics, i.e, the CamVid (Brostow et al. 2008), Freiburg Forest (Valada et al. 2017a) and Gatech (Raza et al. 2013) semantic segmentation datasets.

Network efficiency is a crucial aspect to multiple tasks, especially for robotics applications, due to computational limits on embedded hardware. Thus, we further improve on the efficiency of the approach by compressing the proposed architecture. We performed a set of experiments providing runtime values of our approach on multiple GPUs and investigate the best encoder feature learning block and deep decoder topology to provide the best trade-off between speed and segmentation quality, Section 4.5.9.

The remainder of the paper is organized as follows. We first discuss related work in Section 2. In Section 3, we present an overview of the employed encoder block, propose our new decoder with it correspondent architecture and finally introduce our dynamic weight function for class balancing. Experimental results are reported in section 4. Finally, we summarize our work in Section 5.

## 2 Related Work

We review the recent advances in semantic segmentation using deep neural networks, represented by Fully Convolutional Networks (FCNs). FCNs (Long et al. 2015) are composed by a fully convolutional topology and bi-linear interpolation to perform dense prediction. Following the FCN structure, many works try to alleviate problems related to rough edges segmentation and object vanishing, through exploring context, resolution and boundary alignment. Additionally, we will review efficient network architectures.

Context aggregation and retention of spatial information was explored by dilated convolutions and reduction of down-sampling operations (Yu et al. 2016; L. Chen et al. 2015; L. Chen et al. 2016; Peng et al. 2017). All approaches adopt dilated convolutions to enlarge the receptive field and capture larger contextual information without losing resolution. These methods also reduce the number of downsampling operation, such as pooling, in order to be able to have

higher resolution feature maps at the end of the encoder, helping to produce more crispy edges. Recently, DeeplabV2 proposes Atrous Spatial Pyramid Pooling, which combines features at different fields of view given by a set of dilated convolutions, to include context to a Resnet based encoder. Methods like Zoom-out (Mostajabi et al. 2015) and ParseNet (W. Liu et al. 2015) were designed to incorporate context explicitly. Zoom-out proposes a hierarchical context features network, while ParseNet includes global pooling features to explicitly add context information. Lately, the Global Convolutional Network (GCN) (Peng et al. 2017) incorporates context using large kernels to provide larger receptive fields.

Another set of approaches focusing on recovery of the resolution lost by down-sampling operations are Label Refinement Networks (LRN) (Islam et al. 2017), DeconvNet (Noh et al. 2015), FC-Dense (Jegou et al. 2016) and DPDB-Net (Oliveira et al. 2018). LRNs introduces a multi-resolution refinement approach which solves the problem in a coarse-to-fine fashion by first predicting a low resolution semantic mask, then progressively refining the predictions to get a more detailed result. Each refinement is associated to a resolution related loss to improve information propagation over the network. Deconv-Net introduces an unpooling operation and an hourglass-like network to learn the upsampling process, while FC-Dense replaces the linear convolution operations by densely connected blocks (Huang et al. 2017).

Boundary approaches try to refine the predictions near the object edges. These approaches use the post-processing techniques, such as Adelaide (G. Lin et al. 2016) and bilateral solver (Barron et al. 2016). Adelaide makes use of a CRF built on fully-connected graph, which serves as a boundary refinement after the CNN. Alternative solutions to CRFs are proposed by (Barron et al. 2016; Jampani et al. 2016). (Jampani et al. 2016) proposes the bilateral filter to learn specific potentials within CNNs, providing 10× speed up and comparable performance to CRFs.

A range of studies has focused on exploring efficient convolutional networks that can be trained end-to-end, like Fast-Net (Oliveira et al. 2016), E-Net (Paszke et al. 2016) and SegNet (Badrinarayanan et al. 2015). Fast-Net focuses on pruning over-parametrized layers targeting on efficiency in terms of computational requirements. E-Net introduces a deep convolutional encoder-decoder model with a residual bottleneck structure to build an efficient network architecture.

Different from previous work, we will explore the potential of a new decoder which has a combination of shallow encoder-decoder networks to improve the description power of the proposed network. As highlighted in (Wojna et al. 2017), there is relatively lesser work done on segmentation decoders and it has become a bottleneck. We design an

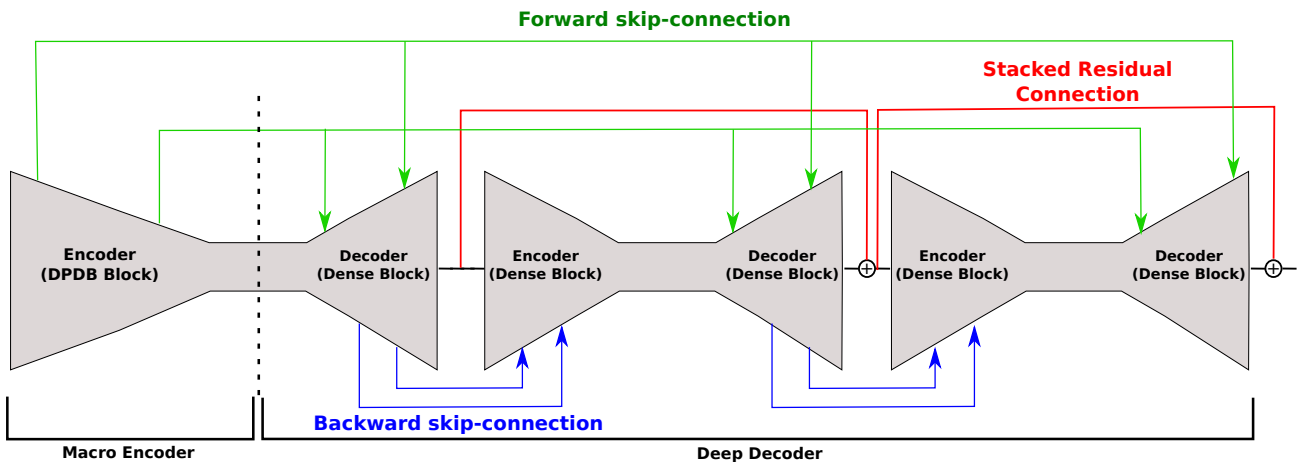


Fig. 1: DD-Net Architecture. Our approach is composed by a macro encoder using DPDB blocks and our deep decoder, composed by sets of decoders-encoders. The main innovations reside in the backward and stacked residual connections. Backward connections aim to explicitly introduce context information to produce more informative features, while the stacked residual targets to enhance the information flow.

architecture to provide the most efficient computational requirement, given its highly deep topology. Additionally our dynamic weight function and deep supervision make our network easy to optimize and capable of producing more discriminative features.

### 3 The Proposed Approach

We propose a decoder that includes multiple shallow networks and new skip connections between encoder-decoder, decoder-encoder, and decoder-decoder. These connections enable better information flow to deeper networks, and give encoders access to higher-level context information. In this section, we provide the details of our proposed method; the full architecture is presented in Figure 1. First, we briefly review the basic DPDB building block in the encoder. Second, we introduce the new decoder block that contains forward, backward, and stacked residual skip connections and deep supervision. Finally, we introduce a weight balancing function which assigns weights dynamically and reinforce under-represented classes.

#### 3.1 Dual Path Dense Block

In a preliminary conference paper (Oliveira et al. 2018), we introduced the dual path dense block (DPDB). It is an efficient subnetwork architecture that incorporates characteristics of feature re-usage and feature exploration to a single block.

#### 3.1.1 Analysis of ResNet and DenseNet

DPDB is motivated by the strengths and weaknesses of the residual and densely connected topologies (He et al. 2015; Huang et al. 2017), respectively.

Let  $x^l$  be the output of the  $l$ -th layer. Standard CNNs compute  $x^l$  by applying a non-linear transformation  $\phi_l$  to the output of the previous layer  $x^{l-1}$ . The equation  $x^l = \phi_l(x^{l-1})$  defines  $\phi_l$  as a set of operations, such as convolution followed by Exponential Linear Units (ELUs) (Clevert et al. 2016) and dropout. Residual networks introduced the so-called *residual block* in order to ease the training of very deep architectures. The residual block sums the input and output layers:

$$x^l := \phi_l(x^{l-1}) + x^{l-1}, \quad (1)$$

making feature reuse possible and permitting gradients to flow directly to early layers. By sharing features across all steps, *residual blocks* encourage feature re-usage and thus reduce feature redundancy. This makes it more difficult for residual networks to explore new features. For residual blocks,  $N_l$  is usually defined as the repetition of  $t$  blocks, usually two, composed by batch normalization, ReLU and convolution.

While *residual blocks* repeat few blocks that are sequentially connected, DenseNets extend this idea with another type of architecture. Dense blocks recursively concatenates all previous feature outputs. The output  $x_l$  of a DenseNet layer is defined as:

$$x^l := N_l([x^{l-1}, x^{l-2}, x^{l-3}, \dots, x^0]), \quad (2)$$

where each layer is a composition of all previous ones through concatenation  $[\dots]$ . The main characteristic of densely connected blocks is the ability to explore new information from previous outputs (Y. Chen et al. 2017). Hence, different features may extract the same information multiple times, leading to a high redundancy block.

The residual network’s main limitation is its summation operation for fusing information. This operation may squash useful features from preceding layers. The squashing problem can be interpreted as follows: given two vectors of weights  $\mathbf{w}_1 \triangleq [w_{11}, \dots, w_{1n}]$  and  $\mathbf{w}_2 \triangleq [w_{21}, \dots, w_{2n}]$  and an element-wise aggregation function  $f_{ag}(\mathbf{w}_1, \mathbf{w}_2) \triangleq \mathbf{w}_1 + \mathbf{w}_2$ , thus, if  $w_{1j} \gg w_{2j}$  then  $f_{ag}(\mathbf{w}_1, \mathbf{w}_2) \sim \mathbf{w}_1 + \boldsymbol{\epsilon}$  then the importance of the low magnitude weights vanishes. Additionally, its high number of parameters, makes very deep residual networks intractable. DenseNets on the contrary can provide a better efficiency in term of parameter usage considering the block operations. On the other hand, dense blocks have an excessive parameter growth, due to the characteristic of successive dense blocks always incorporate the full feature size of the input to compose the new output feature map, which limits the width of DenseNets.

In the following section we will present the Dual-Path Dense-Block (DPDB) approach which combines the advantages of both architectures in a single block.

### 3.1.2 DPDB Block

Based on the previous analysis, we propose a new dense block called Dual-Path Dense-Block. Our block is different from the dual path network (Y. Chen et al. 2017), which also combines concepts from ResNet and DenseNet: we give similar weights to each of the sides and do not use a residual block as main block adding a thin densely connect path.

Given  $x_{l,R}$  and  $x_{l,D}$  as the outputs for the  $l$ -th layers of the residual path and dense path, we formulate the DPDB path block as:

$$x_{l,R} := f_l^r(x_{l,R}^t) = x_{l,R}^{t-1} + \phi_l^r(x_{l,R}^{t-1}), \quad (3)$$

$$x_{l,D} := \sum_{t=0}^{l-1} N_l^t([x_{l,D}^t]), \quad (4)$$

$$r_l := [x_{l,R}, x_{l,D}], \quad (5)$$

$$h_l := G_l(r_l), \quad (6)$$

where  $f_l^r$  and  $N_l^t$  are the feature learning function. Equation 3 refers to the residual path that enables feature re-usage and Equation 4 to the densely connected path that enables new feature exploration. Equation 5 defines the path that fuses the outputs and feeds them to the final transformation function in Equation 6. The transformation function  $G_l(\cdot)$  is responsible for making the next mapping or prediction. Path fusion is done by concatenation to avoid the feature squashing problem.

A full description of the proposed block is depicted in Figure 2. The block consists of two paths that pass through a bottleneck layer. The latter consists of batch normalization, ELU activation function and convolution, followed by a 3x3 kernel layer and finally to a output dimension specific layer. The output is then split into its corresponding path which will employ the specific aggregation functions.

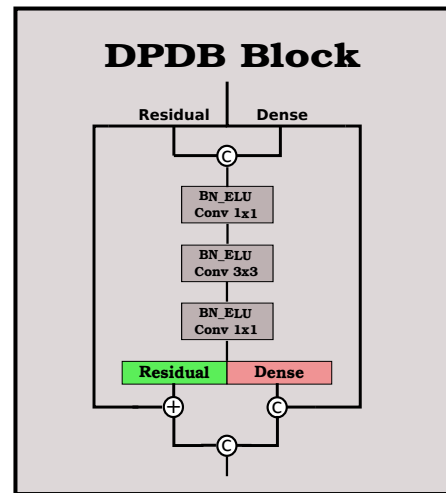


Fig. 2: DPDB block. Dual-Path Dense-Block (DPDB) is a feature learning approach which incorporates feature re-usage (Residual Block) and new feature exploration (Dense Block) into a single learning scheme. BN stands for batch normalization and ELU for exponential linear unit.

## 3.2 Deep Decoder

We propose a new decoder topology, which aims to recover high-resolution predictions through a set of multiple shallow encoder-decoder networks, as shown in Figure 1. Each set of networks are piled up from end-to-end, and forward, backward, and stacked residual connections are jointly employed. The structure of each set consists of a decoder-encoder which adopts Dense Blocks and three upsampling blocks followed by three downsampling ones. In order to further improve information flow and discriminability in the network we deeply supervise all the last units of the decoder block.

### 3.2.1 Skip Connections

The architecture makes use of three different skip connections, namely forward, backward and stacked residual. Forward skip connections are responsible for associating features from the first encoder to all subsequent decoders, backward connections link two adjacent decoder-encoder units

while the stacked residual connections work like macro residuals between decoders.

The first type of skip connection is the standard forward one. Forward skip connections connect parts of the encoder with its respective same resolution decoder counterpart, this is useful given the mid-level representations from the first encoder not pass through a series of downsampling operation that usually reduces its spatial visual information. Thus, such connection promotes the inclusion of less corrupted spatial information and consequently produces better detailed boundaries predictions. The skip-connection operation consists of feeding the features from the layer  $n^{\text{th}}$  of first encoder into a convolutional layer to reduce the number of feature maps to  $F_1^n$ . The reduced features  $F_1^n$  are then aggregated to the output of the upsampling operation through concatenation. The upsampling operation is composed by a transposed convolution followed by a Dense Block, further discussion about this choice is done in Section 4.5.3.

The second type of connection is the backward skip connection, which is inspired by (H. Abdunabi et al. 2017). The authors proposed a connection from late convolutions to early convolution layers in order to enable the early convolution layers understand the context earlier and, thus, being able to adaptively extract more informative features. (H. Abdunabi et al. 2017) proposed a master-slave network where the master network is responsible for producing the label prediction while the slave only provides the backward skip connections to the master’s earlier layers. Their skip connection suffers from a major drawback, which is the doubling of computational costs. Our backward skip connection has similar effects, but with a much smaller computational burden. Instead of a master-slave architecture, we use a set of encoder-decoder networks, where each new encoder in the macro decoder block has backward skip-connections from its previous decoder. This promotes the flow of high-level semantic information to succeeding encoder layers, improves the encoder optimization, and, consequently, makes the context to be captured early on these parts of the network. We adopt three backward connections between every decoder-encoder of DD-Net, using element-wise summation as aggregation function. Three skip connections are related to the three blocks used in each encoder, which are consequently related to the 8x dimensionality reduction which occur at each of the modules.

Along with forward and backward connections we install skip connections between all the high resolution outputs of each decoder. We call this Stacked Residual Connection (SRC). The main goal of SRCs is to act like a macro residual connection between each encoder-decoder set and additionally to produce a multi-stage segmentation mask prediction. From the second decoder on we consider the  $n^{\text{th}}$  final decoder layer, the output  $F_i^n$  are fused with features  $F_i^{n-1}$  from the previous final decoder layer by element-wise

summation to produce a new fused feature  $\bar{F}_i^n = F_i^n \oplus F_i^{n-1}$  which then serve as input to the next encoder-decoder block. Such connection can enhances information flow and improve segmentation results.

### 3.2.2 Deep Supervision

Deeper architectures can potentially produce better results, yet with deeper networks comes the issue of gradient propagation. Skip-connections, like backward and stacked residual, can improve the information flow, but does not completely mitigate such problem. In order to further reduce this problem, we make use of deep supervision (L. Wang et al. 2015).

Deep supervision consists of adding auxiliary supervision branches after certain intermediate layers during training. One of the key aspects of deeply supervised training is where to add the supervision branches. We add auxiliary supervision to the end of each decoder block. The combined loss function for the whole network is then composed by  $K$  auxiliary losses and a main loss, where  $K$  is the number of decoder minus one.

### 3.3 Dynamic Weight Function

Semantic segmentation tasks often come with an uneven distribution of classes in images. A possible solution to class balancing is provided by weight functions. Weighting functions are responsible for providing a new class distribution to the cross-entropy loss in order to make all classes equally important. One strong characteristic from most segmentation input images is the usually low number of instances of a single class per example. Thus, smaller objects will most probably be less represented per sample. This trait motivated the introduction of a new weight function that reweights the class distribution to improve the network attention to these classes, which are often neglected by approaches which consider each class equal in importance.

Median frequency (Eigen et al. 2015) have become the standard method to produce balanced weights for semantic segmentation. However effective for some segmentation problems, it requires to access the whole dataset prior to training and produces a static weight distribution to every sample. This limits its application domain and performance.

Thus, we propose a novel weight function, which assigns weights dynamically, does not need any pre-processing step, and reinforces classes that are under-represented by standard class balancing approaches. We aim to produce a set of weights that are a trade-off between dominant classes and less-represented ones. Our function gives an inverse weight

using as base the class pixel frequency, i.e., smaller objects will have higher weights:

$$DW_i = \frac{C_b + \sum_{i=1}^N C_i}{C_i} \quad (7)$$

where  $N$  is the number of classes,  $C_b$  is the number of background pixels in the image and  $C_i$  the number of pixels of the class  $i$ .

The downside of this function is that frequent classes drop in performance. To restrict this effect, we limit the weight to always be greater than a constant  $L$ :

$$DW_{bounded,i} = \max(DW_i, L) \quad (8)$$

where  $DW_{bounded,i}$  is the lower-bounded weight for class  $i$ , thus we can guarantee no class weight is smaller than one since we further divide  $DW_{bounded,i}$  by  $L$ . We set the background weight always to zero.

## 4 Experiments

We evaluated the performance of our network on three common robotics datasets, CamVid dataset (Brostow et al. 2008), the Freiburg Forest dataset (Valada et al. 2017a) and the Gatech context dataset (Raza et al. 2013). The implementation was based on the publicly available TensorFlow learning toolbox [1] and all experiments were carried out on an NVIDIA Titan X GPU.

For the compared datasets, we report quantitative results and benchmark them with state-of-the-art baselines. We present an in-depth ablation study related to the impact of feature learning at the decoder, class balance approaches, depth of the proposed decoder and network pre-training.

Moreover, we conducted experiments studying the impact of deep decoders to state-of-the-art segmentation techniques, quantifying the gain of using our approach as decoder. As a final set of experiments augmenting semantic segmentation with optical flow information is presented.

### 4.1 Architecture and training details

The network was trained end-to-end using the Adam solver (Kingma et al. 2014) with an initial learning rate of  $2 \times 10^{-4}$  which decay  $10 \times$  every  $2 \times 10^5$  iterations. All models were trained on data augmented images with multi-window random crop and vertical flip. We also applied mean subtraction to images and weight class balancing and regularized our model with a weight decay of  $10^{-4}$  and a dropout rate of 0.1. The mean IoU was monitored every 100 iterations.

### 4.2 CamVid dataset

CamVid is a dataset of fully segmented videos for semantic segmentation of urban environments (Brostow et al. 2008). The dataset is constituted by 367 frames for training, 101 frames for validation and 233 frames for testing. Each frame has  $360 \times 480$  pixels, which are labeled with 11 semantic classes. We trained our network with augmented frames and fine-tuned using a model pre-trained on Cityscapes. The impact of these design choices is quantified in the ablation study in Section 4.5.

The results are summarized in Table 1. As shown in the table, CamVid is an actively benchmarked dataset, the compared methods range from FCNs with dilation convolutions like (Yu et al. 2016), networks with Dense Blocks such as FCDenseNet (Jegou et al. 2016), with additional training data (Richter et al. 2016) to even deeper architectures like SDN (Fu et al. 2019). From all the compared methods only SDN was capable of surpassing 70 percentage points of intersection over union. Our approach not only outperforms SDN and defines the new state-of-the art on CamVid, but DD-Net also uses five times fewer parameters than SDN.

Qualitative results are shown in Figure 3. The first row shows examples in which the segmentation approach performs accurately, however, the tree class is over-segmented. The second and third rows show one of the strongest characteristics of our architecture, namely the highly detailed segmentation of challenging classes, such as person, pole and sign. The last row shows an example with less detailed structures and highlights the common confusion between sky and vegetation, which can be noticed in the fourth row, top-right side. The most common mistake of our approach is also presented in the last three rows, which is the confusion between the car hood and road. This is likely because the hood reflects the road image in most of the examples.

### 4.3 Gatech dataset

Gatech is a scene understanding dataset that consists of 63 training videos and 38 testing videos (Raza et al. 2013). It is much larger than Camvid, with 12000 and 7000 training and testing images respectively. However the annotations are often erroneous. Each video has between 50 and 300 frames, which are divided into 8 classes: sky, ground, buildings, porous, humans, cars, vertical mix and main mix. One difference of evaluation metric is that given the dataset was originally designed to learn 3D geometric structure of outdoor video scenes the standard metric for this dataset is mean global accuracy.

We pretrained our architecture on Cityscapes, as shown in Section 4.5.7. We also provide results with training from scratch. In Table 2, we report the obtained results. As shown in the table, we outperform the compared methods not only

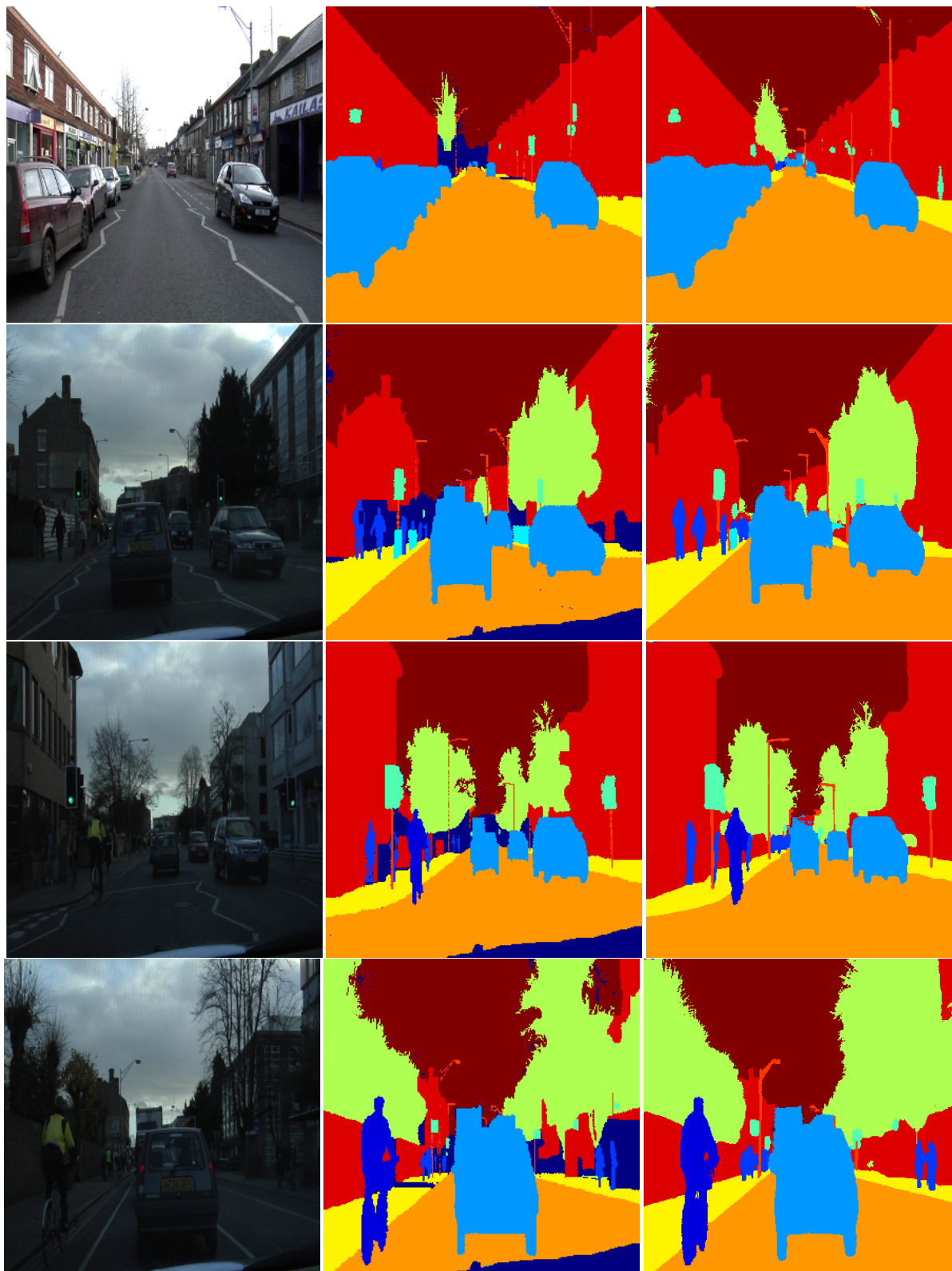


Fig. 3: Qualitative results on the Camvid test set. The rows represent from left to right: Input image, ground truth and prediction of our approach. The first row exemplify a high quality segmentation with only a small inconsistency for the over-segmented tree class. The second and third rows show the higher performance obtained by DD-Net to fine classes, like pole, person and sign. The last row presents another prediction mistake, which is made between sky and vegetation, which happens in the top-right corner. The most common mistake of our approach is between the car hood and road. Such problems happens due to the reflection of the road image in the car hood.

Table 1: Results on CamVid dataset. Our approach obtained an average mIoU of 73.2 percentage points, constituting the new state-of-the-art for the present dataset. Additionally, we only require one fifth of the number of parameters of the second best method.

Method	Parameters (M)	Building	Tree	Sky	Car	Sign	Road	Pedestrian	Fence	Pole	Sidewalk	Cyclist	Global Acc.	mIoU
S.parsing (Tighe et al. 2010)	—	70.4	54.8	83.5	43.3	25.4	83.4	11.6	18.3	5.2	57.4	8.9	—	42.0
ALE (Ladicky et al. 2009)	—	73.4	70.2	91.1	64.2	24.4	91.1	29.1	31.0	13.6	72.4	28.6	—	53.6
Liu (B. Liu et al. 2015)	—	66.8	66.6	90.1	62.9	21.4	85.8	28.0	17.8	8.3	63.5	8.5	—	47.2
SegNet (Badrinarayanan et al. 2015)	29.5	68.7	52.0	87.0	58.5	13.4	86.2	25.3	17.9	16.0	60.5	24.8	62.5	46.2
DeconvNet (Noh et al. 2015)	252	—	—	—	—	—	—	—	—	—	—	—	85.9	48.9
FCN8s (Long et al. 2015)	134	77.8	71.0	88.7	76.1	32.7	91.2	41.7	24.4	19.9	72.7	31.0	88.0	57.0
STFCN (Fayyaz et al. 2016)	—	73.5	56.4	90.7	63.3	17.9	90.1	31.4	21.7	18.2	64.9	29.3	—	50.6
Reseg (Visin et al. 2016)	—	—	—	—	—	—	—	—	—	—	—	—	88.7	58.8
LRN (Islam et al. 2017)	—	—	—	—	—	—	—	—	—	—	—	—	—	61.7
Bayesian SegNet (Kendall et al. 2015)	29	—	—	—	—	—	—	—	—	—	—	—	86.9	63.1
DeepLab-LFOV (L. Chen et al. 2015)	37.3	81.5	74.6	89.0	82.2	42.3	92.2	48.4	27.2	14.3	75.4	50.1	—	61.6
Dilation (Yu et al. 2016)	140	82.6	76.2	89.0	84.0	46.9	92.2	56.2	35.8	23.4	75.3	55.5	79.0	65.3
FCCN (Wu et al. 2017)	—	79.7	77.2	85.7	86.1	45.3	94.9	45.8	<b>69.0</b>	25.2	86.2	52.9	—	65.7
Kundu (Kundu et al. 2016)	—	84.0	77.2	91.3	85.6	49.9	92.5	59.1	37.6	16.9	76.0	57.2	—	66.1
FC-DenseNet103 (Jegou et al. 2016)	—	83.0	77.3	93.0	77.3	43.9	94.5	59.6	37.1	37.8	82.2	50.5	91.5	66.9
DCNN (Fu et al. 2017)	—	—	—	—	—	—	—	—	—	—	—	—	91.4	68.4
G-FRNet (Amirul Islam et al. 2018)	—	83.7	77.8	92.5	83.6	44.7	94.6	58.4	45.2	34.7	83.2	58.1	—	68.8
Playing for data (Richter et al. 2016)	—	84.4	77.5	91.1	84.9	51.3	94.5	59.0	44.9	29.5	82.0	58.4	—	68.9
SDN (Fu et al. 2019)	161	85.2	77.5	92.3	<b>90.2</b>	<b>53.9</b>	96.0	63.8	39.8	38.4	85.3	66.9	92.7	71.8
DD-Net	31.6	<b>85.3</b>	<b>79.4</b>	<b>93.0</b>	86.7	51.4	<b>96.7</b>	<b>68.5</b>	41.1	<b>44.6</b>	<b>88.0</b>	<b>70.4</b>	<b>93.1</b>	<b>73.2</b>

in the fine-tuned scenario but also when the network is trained from scratch, even methods which include temporal consistency like (Tran et al. 2016) and (Y. Wang et al. 2017) cannot produce as accurate results as the proposed technique. Figure 4 presents qualitative results for the tested dataset, mainly showing that however with poorly annotated labels our technique can still produce good predictions.

Table 2: Results on Gatech dataset. The results are divided into trained from scratch and pre-trained. For both settings we outperform the current methods, even when compared to approaches which use temporal information.

Method	Temporal Info	Acc.
2D-V2V-scratch (Tran et al. 2016)	No	55.7
3D-V2V-scratch (Tran et al. 2016)	Yes	66.7
DD-Net-scratch	No	<b>72.7</b>
3D-V2V (Tran et al. 2016)	Yes	76.0
FC-DenseNet103 (Jegou et al. 2016)	No	79.4
HDCNN (Y. Wang et al. 2017)	Yes	82.1
DD-Net	No	<b>83.1</b>

Table 3: Results on Freiburg Forest dataset. Our proposed network outperform all the previous approaches, even when compared to a strong baselines which even use the same feature learning block at the encoder like DPDB-Net (Oliveira et al. 2018).

Method	Sky	Trail	Grass	Veg	mIoU
FCN (Long et al. 2015)	—	—	—	—	77.0
ParseNet (W. Liu et al. 2015)	87.7	81.8	85.2	85.2	85.0
E-Net (Paszke et al. 2016)	—	—	—	—	71.4
M-Net (Oliveira et al. 2017)	89.2	82.4	84.9	88.7	86.3
Fast-Net (Oliveira et al. 2016)	90.4	84.5	86.7	90.6	88.0
GCN (Peng et al. 2017)	91.9	86.2	86.4	88.7	88.3
DPDB (Oliveira et al. 2018)	92.3	87.2	87.8	90.1	89.4
DD-Net	<b>92.9</b>	<b>88.9</b>	<b>88.5</b>	<b>90.7</b>	<b>90.2</b>

#### 4.4 Freiburg Forest dataset

The Freiburg Forest dataset is an outdoor dataset for unstructured semantic segmentation (Valada et al. 2017a). Unstructured semantic understanding is critical for robots operating in real world scenarios. The dataset is composed by 325 frames with pixel-level annotation, which has 203 frames for training and 122 frames for testing. The groundtruth is

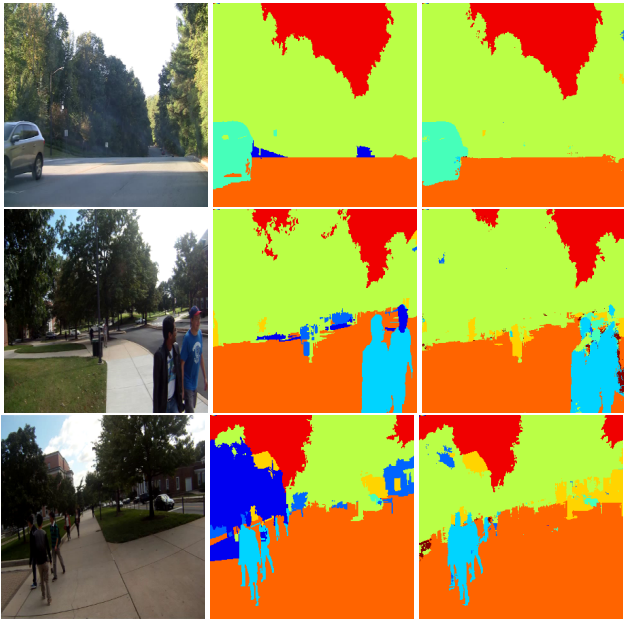


Fig. 4: Qualitative results on the Gatech dataset. The rows represent from left to right: input image, ground truth and prediction of our approach. The first row shows good segmentation, with small false positive detection cases. The second and third examples count with poorly annotated masks that directly reflect on the segmentation predictions. For instance in the second row the right most person’s head is wrongly annotated. Even with the presented problem our approach is still capable of segmenting classes like humans, ground, cars and sky correctly.

divided into five classes, such as sky, trail, grass, vegetation and obstacle.

Table 3 reports the obtained state-of-the-art results and comparisons to the baseline. The experiment comprises an interesting comparison between our method and the previous state-of-the-art approach which uses an encoder with the same feature learning block. Such result displays that our decoder can further improve segmentation, even for a dataset which presents high performance results already. Another key aspect of our method, that is interesting for robotics applications, is the high IoU value for the traversable area of the dataset, namely trail class. High fidelity traversability prediction is of great interest for robotic path planning algorithms. Figure 5 presents multiple segmentation examples of our method for the Freiburg Forest dataset.

#### 4.5 Ablation Studies

The performance of different components, like block learning, new blocks to encoder, decoder feature learning, decoder depth, skip-connections, class balancing, network pre-

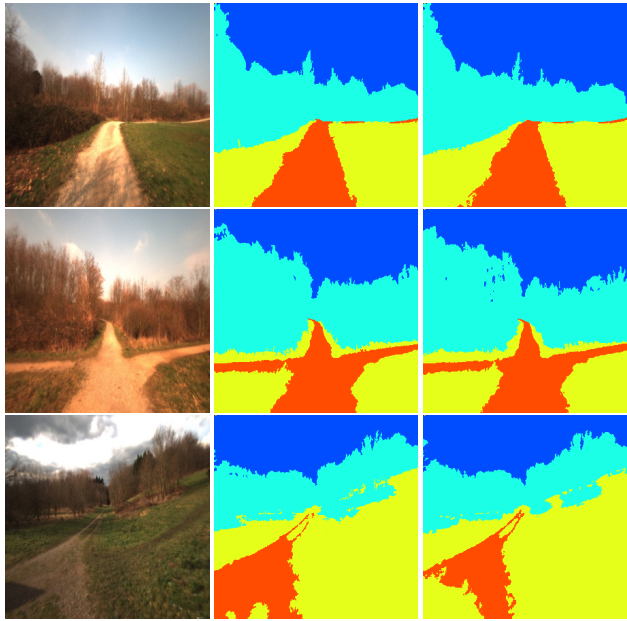


Fig. 5: Qualitative results on the Freiburg Forest test set. The rows represent from left to right: Input image, ground truth and prediction of our approach. The first row depicts a good segmentation example with high quality segmentation mask. The second row exemplify a multi-path segmentation situation. The last row presents a sample of bad segmentation produced by our approach.

training and deep decoders to modern networks will be presented in the following sections. All ablation studies until Section 4.5.7 are trained from scratch to provide a cleaner baseline comparison. We quantify the incremental performance of each component, which lead to our final approach.

##### 4.5.1 Block learning analysis

An analysis of the choice between the deployment of DPDB blocks over dense blocks is presented in Table 4. We have tested three different settings, single encoder-decoder using only dense blocks, single encoder-decoder with DPDB blocks for the encoder and dense blocks for the decoder and our full approach with DPDB blocks for the encoder and dense blocks for the deep decoder. For single encoder-decoder approaches we can notice that using DPDB blocks can produce a gain superior to five percentage points over its dense block counter-part. While single encoder-decoder architectures perform well, the gap of performance between them and a multiple stage decoder, in our case superior to 10.8 percentage points, makes deep decoders an interesting design choice for future semantic segmentation networks.

Table 4: Ablation study with Dense and DPDB blocks. Results using the CamVid dataset. The experiment confirm the superior results of DPDB blocks for feature learning when compared to Dense Blocks in a single encoder-decoder setting. The experiment also quantify the gain of replacing a single decoder by our deep decoder approach.

Method	Building	Tree	Sky	Car	Sign	Road	Pedestrian	Fence	Pole	Sidewalk	Cyclist	Global Acc.	mIoU
Dense blocks encoder-decoder	66.9	62.4	81.1	45.5	28.8	83.2	38.9	26.8	22.5	62.0	22.4	81.0	49.1
DPDB encoder single decoder	72.4	62.9	88.6	61.9	30.0	88.8	44.8	26.1	23.6	69.4	33.1	85.2	54.7
DD-Net	<b>80.4</b>	<b>74.0</b>	<b>92.1</b>	<b>78.8</b>	<b>41.3</b>	<b>94.5</b>	<b>56.9</b>	<b>25.7</b>	<b>34.1</b>	<b>80.7</b>	<b>61.8</b>	<b>90.4</b>	<b>65.5</b>

Table 5: Ablation study about the impact of feature learning after upsampling. Results using the CamVid dataset. The experiment shows the importance of learning the upsampled features. Only upsampling displays the worst values. Standard upsampling followed by a convolution operation is outperformed by upsampling with a better feature learning approach, in our case upsampling followed by a Dense block.

Method	Building	Tree	Sky	Car	Sign	Road	Pedestrian	Fence	Pole	Sidewalk	Cyclist	Global Acc.	mIoU
Only upsampling	78.5	72.8	91.7	75.3	37.5	93.7	54.5	22.7	30.4	78.9	50.9	89.5	62.4
Convolution after upsampling	80.0	<b>74.2</b>	91.7	77.0	39.7	93.1	54.7	22.3	32.8	77.7	56.5	89.9	63.6
DenseBlock after upsampling	<b>80.4</b>	74.0	<b>92.1</b>	<b>78.8</b>	<b>41.3</b>	<b>94.5</b>	<b>56.9</b>	<b>25.7</b>	<b>34.1</b>	<b>80.7</b>	<b>61.8</b>	<b>90.4</b>	<b>65.5</b>

#### 4.5.2 New blocks to DD-Net

Different learning blocks can incorporate new characteristics to segmentation. This setting is constituted by replacing the macro encoder by a new encoder with similar topology but with a different feature learning block. In the following experiments we used inverted residual blocks (Sandler et al. 2018) and Dense blocks (Huang et al. 2017). We choose inverted residual blocks based on its recent results on the MobileNet v2 architecture, which is a modern instance of efficient feature learning block. Additionally to inverted residual block we also use Dense blocks for further comparison. Table 6 summarizes the results of the three tested configurations on the CamVid dataset.

The results show that inverted residual blocks and dense blocks while well known efficient blocks are still not capable of surpassing our DPDB block in the same setting. Both inverted residual and dense blocks are performing around 62 mean IoU percentage points, with a 0.6 percent advantage to dense blocks. The only exception is the class fence where the inverted residual version is the highest IoU among the tested configurations. Our full approach with DPDB blocks at the decoder and deep decoders perform the highest with a mean IoU gain over the baselines by 2.8 percentage points. This result again confirm the power of Dual-Path Dense-Blocks for feature learning in semantic segmentation tasks.

#### 4.5.3 Feature Learning at Decoder

The impact of operations after upsampling features is explored in this section. We analyze the impact of no convolution after transposed convolution, convolution and dense-blocks after the upsampling operation. Table 5 summarized our obtained results where having a Dense Block after a transposed convolution can produce a gain of 3.1 percentage points over only upsampling and a gain of 1.9 percentage points over the standard strategy of including a convolution layer after the upsampling operation. The better feature representation given by Dense Blocks and the lack of residual connections which can potentially squash features, see Section 3.1.1, makes it the best candidate to learn upsampled feature at the decoder part.

#### 4.5.4 Depth of Decoder

The following experiments aim to understand the impact of the number of connected decoder-encoder units to the network’s performance. The key feature we target to incorporate is that each included unit can capture more contextual information and produce higher fidelity predictions. To validate this goal, we trained multiple networks which gradually increase the number of units until we face memory limitations to further increment. The tested topologies are presented in Table 7. The observed results show a consistent performance improvement with the growth of the decoder-encoder units, respectively we got a increment of 1.1 per-

Table 6: Ablation study about the impact of learning blocks to DD-Nets.

Method	Building	Tree	Sky	Car	Sign	Road	Pedestrian	Fence	Pole	Sidewalk	Cyclist	Global Acc.	mIoU
Inverted Residual + DD	77.8	73.2	91.2	77.3	36.0	93.4	49.6	<b>26.0</b>	31.2	77.8	49.9	89.3	62.1
Dense block + DD	78.9	72.3	91.5	75.4	37.5	93.2	53.6	24.6	30.9	78.4	53.6	89.5	62.7
DPDB block + DD	<b>80.4</b>	<b>74.0</b>	<b>92.1</b>	<b>78.8</b>	<b>41.3</b>	<b>94.5</b>	<b>56.9</b>	25.7	<b>34.1</b>	<b>80.7</b>	<b>61.8</b>	<b>90.4</b>	<b>65.5</b>

Table 7: Decoder depth experiments on CamVid. The experiments indicate that, with increasing number of decoder blocks, the model benefits from the deeper network.

Method	Building	Tree	Sky	Car	Sign	Road	Pedestrian	Fence	Pole	Sidewalk	Cyclist	Global Acc.	mIoU
One Decoder Block	80.3	72.9	91.8	77.0	40.2	94.2	52.9	24.7	32.8	80.3	53.3	90.2	63.7
Two Decoder Blocks	<b>80.9</b>	73.7	91.9	78.1	<b>41.4</b>	94.4	55.1	25.6	33.7	80.5	58.2	<b>90.5</b>	64.8
Three Decoder Blocks	80.4	<b>74.0</b>	<b>92.1</b>	<b>78.8</b>	41.3	<b>94.5</b>	<b>56.9</b>	<b>25.7</b>	<b>34.1</b>	<b>80.7</b>	<b>61.8</b>	90.4	<b>65.5</b>

centage points in the IoU metric from one to two decoders and 0.7 percentage points from two to three units. The main gains are obtained by the least frequent and more complex classes, namely pedestrian and cyclist. Pedestrian exhibits an 4 percentage points improvement while the class cyclist presents the largest improvement of 8.5 percentage points between one and three units. Qualitative results with the different settings are presented in Figure 6.

The results shown in Figure 6 mainly exemplify the false positive detection reduction with the decoder depth increment. The first column shows the specific case of the building class, the bottom left area presents multiple false positive regions, which are reduced with the increment of units. The second column is a sample of the better segmentation of the car class, holes are gradually closed, producing a boost of 1.8 percentages points for this class. Column three is another example of the reduction on false-positive detections, where more units can reduce such occurrence.

#### 4.5.5 Skip-connections and resolution

This section is dedicated to quantify the effect of each type of skip connection and their combination. Additionally, we investigate the impact of resolution input to the network’s segmentation accuracy. The first experiments quantify the impact of only forward skip-connections, with a combination of forward and backward, forward and residual and with our complete approach which is composed by forward, backward and residual connections. Table 8 presents the obtained results. The experiment confirms the hypothesis that backward and residual connections can improve context information flow and consequently produce better segmentation masks. The FBR (Forward-Backward-Residual)

model shows a considerable gain over the other settings. The Camvid and Freiburg Forest datasets also support this finding. Only on the Gatech dataset the inclusion of the backward and residual skip-connections has a negative impact in the network’s segmentation quality metric. After verifying results qualitatively, we believe that the network actually performs better with the additional skip-connections (as on the other datasets), but suffers from the noisy annotation in the quality metric. Figure 4 shows an example in the middle row, where DD-Net produces a consistent prediction to the person class, yet the (wrong) annotation assigns it to the background.

We further extend our experiments to test different resolutions. The resolutions include images from  $300 \times 300$  to  $360 \times 360$ . Table 9 summarizes the results for both resolutions on CamVid dataset. Higher resolution inputs have the positive aspect of producing higher resolution segmentation masks at the end of the encoder and consequently a better defined initial segmentation prediction. As shown in our experiment increasing the resolution produces better results for all classes, outperforming all the previous tested settings.

#### 4.5.6 Class balance experiments

Class imbalance is a natural characteristic of several segmentation datasets, causing two problems: (1) approach focus on more frequent classes that contribute to no useful learning signal of all classes; (2) easily classified classes can produce bias and degenerate models. Some approaches aim to solve such problem with median frequency class balance (Eigen et al. 2015) or Focal Loss (FL) (T. Lin et al. 2017). Median frequency class balance computes over the whole dataset a set of static weight classes given by  $ac =$

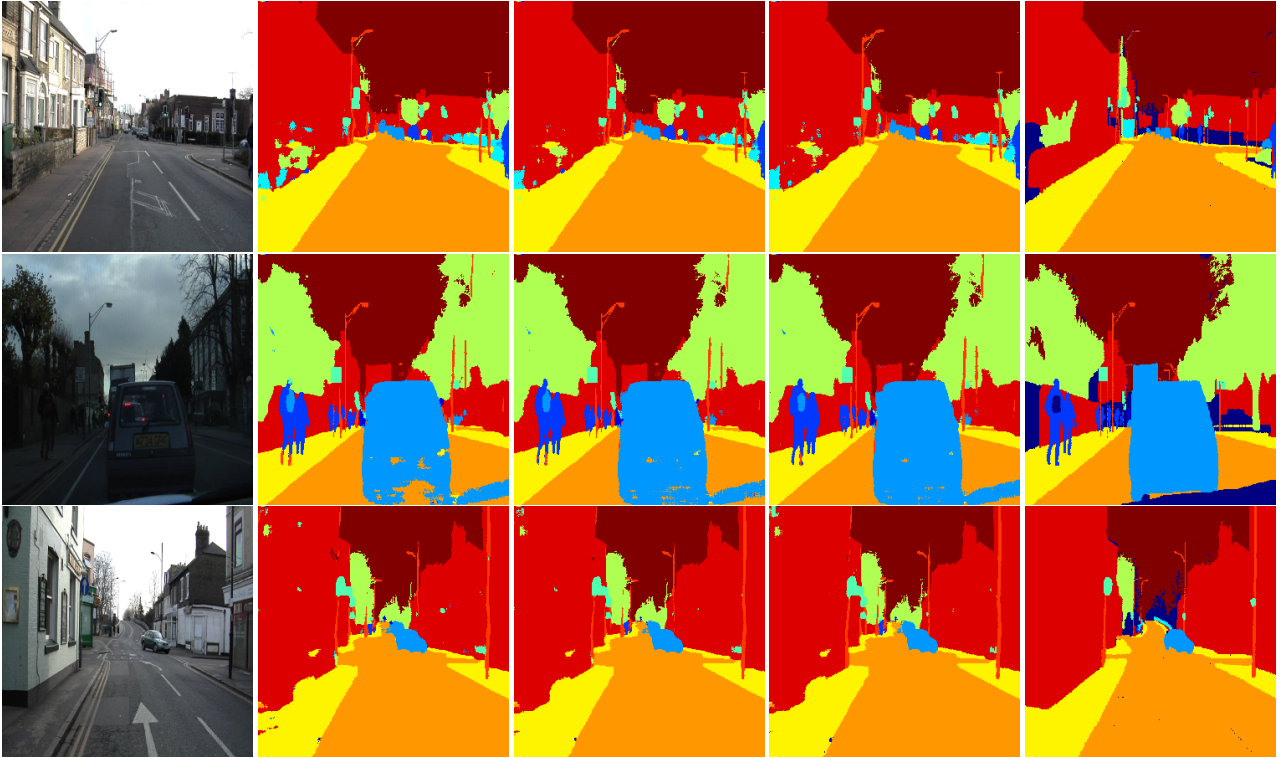


Fig. 6: Depth of decoder experiments. The columns show from left to right: Input image, result of the one-unit decoder, result of the two-unit decoder, results of the three-unit decoder and ground truth. What can be seen is the reduction of false-positive prediction with more units at the decoder. For instance the car class in the middle row presents gradually less holes.

$median\_freq/freq(c)$ . Class specific frequency  $freq(c)$  is the total number of pixels in images where  $c$  is present, and median frequency is the median of these frequencies. Focal loss is a dynamic scale weight function to the cross entropy loss. The aim is to reshape the loss function to down-weight easy examples and consequently focus training on hard examples. Focal loss cross entropy is designed to binary classification, however we implement an  $\alpha$ -balanced multi-class implementation based on the Equation 9.

$$F_L(p_t) = -\alpha_t (1 - p_t)^\gamma \log(p_t) \quad (9)$$

where  $p_t \in [0, 1]$  is the model’s estimated probability for the class  $t$ ,  $\alpha_t \in [0, 1]$  is the corresponding weight factor and  $\gamma \in [0, 5]$  is the focusing parameter. The component  $(1 - p_t)$  is the modulating factor for the cross entropy, which is responsible for adjusting the class weight. Additionally, we also tested our dynamic weight approach using focal loss, see Equation 10. This configuration aims to test how our area centric approach will behave with a decay function. The obtained results are presented in Table 10. The results show that median frequency class balancing and no class balancing present similar results. For the focal loss experiment the results deteriorate when compared to the other settings, even

when dynamic weight is included the obtained values are inferior to our sole weight function. The probable limitation of focal loss approaches is the aggressive change on the distribution of the values. Our approach, different from focal loss, does not change the class weights for the same input over time and consequently does not present such limitation.

$$F_L(p_t) = -\alpha_t DW_{bounded,t} (1 - p_t)^\gamma \log(p_t) \quad (10)$$

#### 4.5.7 Network pre-training

Neural networks training usually requires large datasets with ground truth annotations. Data augmentation can alleviate this limitation through geometric and appearance transformation to the current dataset in order to produce more samples. However, presenting positive practical results it still cannot replace the need of thousands of labelled images for optimization. The following experiments will quantify the gains of network pre-training.

Network pre-training constitutes one of the main steps for CNN optimization. Given more diverse datasets, for instance Cityscapes (Cordts et al. 2016) and Imagenet (Deng et al. 2009), fine-tuning on such datasets can further improve performance due to a richer feature representation. In

Table 8: Ablation study on the impact of the different types of skip-connections on three different datasets. F stands for forward connection, B for backward, and R for residual. **Top:** CamVid dataset. **Bottom left:** Freiburg Forest dataset. **Bottom right:** Gatech dataset. The results support the claim that the proposed skip-connections provide a better context information flow which reflects on the quality of segmentation. The only drawback of the inclusion of backward and residual skip connections are in the case of corrupted annotations, for example presented in the Gatech dataset.

Method	Building	Tree	Sky	Car	Sign	Road	Pedestrian	Fence	Pole	Sidewalk	Cyclist	Global Acc.	mIoU
F	79.7	73.2	91.6	78.6	41.2	93.9	54.1	23.3	30.8	80.0	56.4	89.9	63.9
FB	<b>81.0</b>	73.6	92.0	78.0	39.4	93.8	<b>57.6</b>	<b>28.4</b>	31.9	80.1	52.4	90.3	64.4
FR	80.7	<b>74.6</b>	<b>92.1</b>	77.8	39.9	94.0	55.6	24.0	<b>34.6</b>	80.0	56.1	<b>90.4</b>	64.5
FBR	80.4	74.0	<b>92.1</b>	<b>78.8</b>	<b>41.3</b>	<b>94.5</b>	56.9	25.7	34.1	<b>80.7</b>	<b>61.8</b>	<b>90.4</b>	<b>65.5</b>

Method	Sky	Trail	Grass	Veg	mIoU
F	92.7	87.5	87.7	90.3	89.56
FR	92.6	87.6	87.9	90.4	89.65
FB	92.6	87.6	87.9	90.5	89.67
FBR	<b>92.9</b>	<b>88.9</b>	<b>88.5</b>	<b>90.7</b>	<b>90.25</b>

Method	Accuracy
F	<b>81.8</b>
FR	80.9
FB	81.0
FBR	81.2

Table 9: Experiments with varying resolution for our trained from scratch approach on the CamVid dataset. Higher resolution inputs are beneficial.

Method	Building	Tree	Sky	Car	Sign	Road	Pedestrian	Fence	Pole	Sidewalk	Cyclist	Global Acc.	mIoU
DD-Net - $300 \times 300$	80.4	74.0	<b>92.1</b>	78.8	41.3	94.5	56.9	25.7	34.1	80.7	61.8	90.4	65.5
DD-Net - $360 \times 360$	<b>81.5</b>	<b>75.1</b>	<b>92.1</b>	<b>80.1</b>	<b>43.1</b>	<b>95.0</b>	<b>58.8</b>	<b>28.3</b>	<b>35.4</b>	<b>82.2</b>	<b>58.1</b>	<b>91.0</b>	<b>66.3</b>

Table 10: Results with different weight functions for our trained from scratch model on the CamVid dataset. FL mean focal loss cross-entropy. Focal loss alone presented the lowest obtained result. Even when used together with our dynamic weights is still not as accurate as just using solely our approach. We believe the change in the priors induced by the focal loss function is harmful for multi-class learning.

Method	Building	Tree	Sky	Car	Sign	Road	Pedestrian	Fence	Pole	Sidewalk	Cyclist	Global Acc.	mIoU
No Class Balance	<b>81.0</b>	74.5	92.4	<b>80.9</b>	<b>42.4</b>	<b>94.7</b>	<b>58.8</b>	17.8	31.5	80.6	54.6	<b>90.9</b>	64.5
Med. Freq. (Eigen et al. 2015)	79.5	<b>74.7</b>	<b>92.5</b>	79.3	41.3	93.8	54.0	22.8	32.7	78.8	58.8	90.2	64.4
FL (T. Lin et al. 2017)	79.2	73.1	<b>92.2</b>	81.1	38.1	93.6	52.6	24.2	31.2	78.9	59.9	89.2	64.0
FL - Dynamic Weights	80.3	73.9	92.2	79.2	39.6	94.5	55.3	<b>29.7</b>	33.0	80.4	55.0	<b>90.9</b>	64.8
Dynamic Weights	80.4	74.0	92.1	78.8	41.3	94.5	56.9	25.7	<b>34.1</b>	<b>80.7</b>	<b>61.8</b>	90.4	<b>65.5</b>

automotive environments the Cityscapes dataset is a common dataset for such pre-training. It contains 2975 training images and 500 validation images. Cityscapes is a highly challenging benchmark, given the 50 cities with different weather conditions, seasons and many dynamic objects. We adjusted the annotation to match the KITTI and Camvid datasets. Annotations for the modified Cityscapes are: sky,

building, road, sidewalk, cyclist, vegetation, pole, car, sign and pedestrian. Table 11 presents the obtained results training and testing on Cityscapes following the same setting as (Valada et al. 2017b). Our obtained results largely outperform all the compared results, even when compared to the AdapNet, which is a multi-resolution, multi-GPU, residual net based architecture.

Table 11: Comparison of semantic segmentation performance on reduced version of the Cityscapes dataset. The reduced version aim to produce a CamVid like annotation pattern. As seen we outperform the previous state-of-the-art approach by more than eight percentage points, considering mean IoU.

Method	Sky	Building	Road	Sidewalk	Cyclist	Vegetation	Pole	car	Sign	Pedestrian	mIoU
FCN8s (Long et al. 2015)	81.20	77.76	92.80	59.70	49.23	78.80	21.5	76.50	48.84	47.57	63.39
SegNet (Badrinarayanan et al. 2015)	69.93	59.87	83.25	43.35	27.25	68.83	19.23	60.80	23.81	24.14	48.04
ParseNet (W. Liu et al. 2015)	82.21	78.42	92.76	60.78	50.30	79.68	22.86	77.90	49.12	44.65	63.87
AdapNet (Valada et al. 2017b)	<b>87.13</b>	83.14	94.45	68.93	52.36	85.72	39.44	84.16	50.73	47.81	69.39
DD-Net	85.27	<b>88.99</b>	<b>97.22</b>	<b>80.06</b>	<b>67.64</b>	<b>90.32</b>	<b>52.50</b>	<b>91.08</b>	<b>60.94</b>	<b>68.95</b>	<b>78.30</b>

Table 12: Pre-training results on CamVid dataset. The experiment presents a training from scratch vs pre-trained on Cityscapes version of our approach. As depicted our pre-trained model outperform the previous setting by 6.9 mean IoU percentage points.

Method	Building	Tree	Sky	Car	Sign	Road	Pedestrian	Fence	Pole	Sidewalk	Cyclist	Global Acc.	mIoU
DD-Net - Scratch	81.5	75.1	92.1	80.1	43.1	95.0	58.8	28.3	35.4	82.2	58.1	91.0	66.3
DD-Net - Cityscapes FT	<b>85.3</b>	<b>79.4</b>	<b>93.0</b>	<b>86.7</b>	<b>51.4</b>	<b>96.7</b>	<b>68.5</b>	<b>41.1</b>	<b>44.6</b>	<b>88.0</b>	<b>70.4</b>	<b>93.1</b>	<b>73.2</b>

The promising results achieved on the Cityscapes dataset motivated the experiment of using the trained weights on other datasets, for example fine-tuning for the CamVid dataset. Table 12 summarizes the results with and without fine-tuning (FT). Pre-training produces an improvement superior to 6 percentage points in the intersection over union metric, also individually producing gain in all the CamVid classes. Additionally, we also experimented the impact of fine-tuning with different datasets for the Gatech setting. Table 13 presents the impact of pre-training for the dataset, given the low number of samples the model using CamVid weights performs almost 2 percentage points worse than the Cityscapes pre-trained counter-part. The diversity of the learned features from Cityscapes can produce a more generic model which consistently improve the results on all compared datasets.

Table 13: Gatech results without fine-tuning and using CamVid and Cityscapes as pre-trained models. We obtain a gain superior to eight percentage points between training from scratch and using CamVid as initial weights. The presented improvement can be further extended, almost two percentage points, when pre-trained on Cityscapes.

Method	Accuracy
Gatech only	72.7
CamVid+fine-tuning	81.2
Cityscapes+fine-tuning	<b>83.1</b>

#### 4.5.8 Deep Decoder to modern networks

This study aims to measure the impact of deep decoders to modern techniques such as DeepLab v2 (L. Chen et al. 2016) and the DeepLab v3 family (L. Chen et al. 2018). Our goal is to show if our approach can further improve state-of-the-art semantic segmentation methods.

DeepLab v2 is an encoder-decoder architecture which make use of dilated convolution, also know as atrous convolution, to propose a new pyramidal model called Atrous Spatial Pyramid Pooling (ASPP). ASPPs when combined with a fully connected Conditional Random Field (CRF) post processing module can produce improved results. Additionally a multi-scale input technique is designed to further improve the network (Lazebnik et al. 2006). The main contribution resides on the application of atrous convolutions to semantic segmentation, when compared to regular convolution with larger filters, atrous convolution allow to enlarge the field of view without increasing the amount of computation required.

The experimental setting consists of taking Deeplab v2 and reporting results with and without our deep decoder, in order to measure the impact of our method to a standard benchmark architecture. Based on hardware limitations we were unable to use the full DeepLab v2 system, for that situation we use the same settings for both experiments, input resolution of  $256 \times 512$ , batch size of 2, not use multi-scale inputs and no CRF post processing. For the reported results

we are using the full cityscapes dataset and report the obtained results on the cityscapes validation set, see Table 14.

Table 14: Comparison between the DeepLab v2 and DeepLab v2 with our deep decoder. Different from other experiments we are using the full cityscapes dataset and DeepLab v2 pre-trained on ImageNet.

Method	mIoU
DeepLab v2	65.6
DeepLab v2 with DeepDecoder	68.1

The changes to the baseline to include our deep decoder is the addition of forward skip connections between the encoder and the new decoder and a deep decoder with two decoders and one encoder, the full deep decoder is not possible to be implemented due to memory limitations. The Table 14 shows the results obtained after training for 100 epochs and presents a gain of 2.5 percentage points with the inclusion of our deep decoder, which indicates the power of our approach to improve strong baselines like the DeepLab v2 architecture.

The modifications done to adequate DeepLab v2 to include our deep decoder are presented in Figure 7. The changes include the inclusion of three forward skip connections and the deep decoder module.

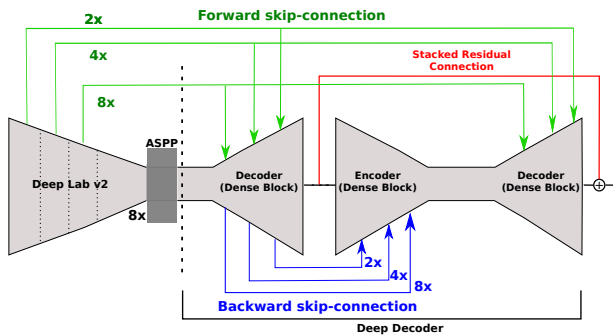


Fig. 7: DeepLab v2 with deep decoder.

The next experiment consists of taking the state-of-the-art DeepLab v3+ model (L. Chen et al. 2018) and report results with and without our deep decoder. DeepLab v3+ is an evolution of DeepLab v3 where the authors proposed an improved version of their ASPP module and new decoder module to refine the segmentation results.

Due to hardware limitations, we were unable to use the same resolution and batch size of the original paper, in this situation we used the same setting for both configurations. The input resolution of  $256 \times 512$ , batch size of 2 and a single scale input approach was used. The reported results are

obtained from training on the cityscapes validation set, Table 15.

Table 15: Comparison between the DeepLab v3+ and DeepLab v3+ with our deep decoder. Different from other experiments we are using the full cityscapes dataset and DeepLab v3+ pre-trained on ImageNet.

Method	mIoU
DeepLab v3+	67.1
DeepLab v3+ with DeepDecoder	68.7

The changes to the baseline to include our deep decoder is the addition of one forward skip connection, at the same way it was implemented originally in the paper. The Table 15 shows the results obtained after training for 100 epochs and presents a gain of 1.6 percentage points with the inclusion of our deep decoder, which confirm the power and generality of our approach to improve strong baselines like the DeepLab v3+ architecture.

The modifications to include our deep decoder to the DeepLab v3+ model are presented in Figure 8. The changes only include the replacement of the DeepLab v3+ decoder module by our deep decoder approach. Table 16 presents the IoU values for each class for the DeepLab v2 and DeepLab v3+ settings. The comparison between DeepLab v2 and the version with the inclusion of the proposed decoder shows the advantage of deep decoders for segmentation. Our approach not only shows a gain in the mean IoU of 2.5 percentage points but also is consistently better for most classes, the only exceptions are the bus and motorcycle classes. Results on DeepLab v3+ quantifying the gain of our approach on the baseline architecture are shown next. The mean IoU gain is around 1.6 percentage points, however some classes like bus, truck and train we outperform the baseline by 10, 11 and 6 percentage points respectively.

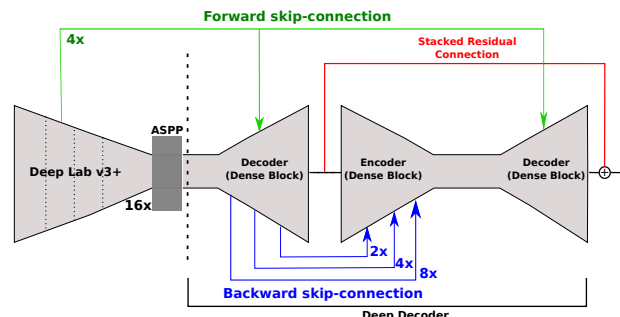


Fig. 8: Deeplab v3+ with deep decoder.

We can conclude from this study that deep decoders shows improvement to semantic segmentation existing tech-

niques. The gains will depend on the topology of the baseline approach, however even for strong baselines like DeepLab v3+ deep decoder are beneficial.

#### 4.5.9 Performance Tests

Deployment runtime is a key aspect of methods which aim to be used into real life or mobile applications. The vast amount of possible hardware options can produce large performance differences. We aim with this study to benchmark our approach on various various GPUs, namely TITAN X, TITAN Xp, GTX 1080 and 180Ti, P100 and TITAN V. We tested five different modern GPUs, see Table 17.

We can notice from this experiment that our approach can be deployed on GPUs with multiple memory sizes, ranging from 8 gigabytes for the GTX 1080 to the 16 gigabytes for the P100 GPUs. The top performing results are obtained on the TITAN V and 1080Ti cards. TITAN V cards can perform a full forward pass in less than 140 milliseconds, constituting a 7 frames per second capability. The slowest setting was using a TITAN X GPU in which a forward pass takes 306 milliseconds on average.

Additionally to the full DD-Net approach, we also experimented focusing on optimizing the runtime of our approach. The first change consists of replacing the DPDB block by inverted residuals in the encoder, however we kept the full deep decoder. The results are obtained using the CamVid dataset and summarized in Table 18. The change between DPDB and inverted residual blocks reduce the need time for a single forward pass by half, nonetheless the mean IoU metric is 3.4 percentage points lower. Such configuration can be important for the deployment of DD-net on robots with low computation capabilities. The new configuration can already provide a 14 frames per second response time. Changing the encoder block gives a substantial saving, related to runtime, but we also experimented reducing the deep decoder size. Following the results from Section 4.5.4 we reduced the size of our deep decoder from three decoder blocks to two decoder blocks. This modification impacted the overall performance by 4.1 percentage points when compared to the full approach, although our technique now only needs 47 milliseconds for a single forward pass, which constitutes a gain of almost three times when compared to our full approach and as consequence a method capable of meeting mobile robots requirements.

#### 4.6 Optical Flow Augmentation for Semantic Segmentation

The majority of semantic segmentation methods rely only on appearance cues and don't exploit other input modalities. Some attempts to include depth were explored recently by (Mousavian et al. 2016; Zhang et al. 2018), nonetheless motion clues have been less explored as an important clue

for segmentation. Motion cues can be a challenging task because of the camera motion along with the motion of independent objects, see Figure 9.

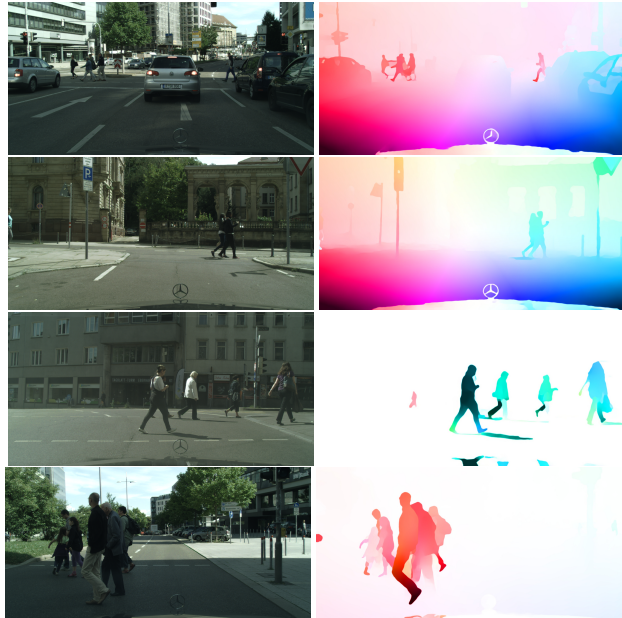


Fig. 9: Image and corresponding flow inputs. The top two rows are examples of optical flow with ego motion flow and independent object motion. The last bottom rows are examples without ego motion on the scene and for consequence easier instances for motion prediction.

Semantic segmentation approaches can benefit from the inclusion of motion clues, optical flow can provide complementary cues about a dynamic scene that can be used to generate richer model of the scene. Additionally motion clues can also be used for semantic motion segmentation, which is the ability of semantic segmentation to classify pixels as dynamic or static.

Attempts to fuse appearance and motion clues have been proposed by (Hur et al. 2016; Jain et al. 2017; Vertens et al. 2017). The work from (Vertens et al. 2017) is a method which uses flow information for semantic motion segmentation, while presenting good results its massive architecture, in terms of memory and gpu requirements, makes it unfeasible to robotics applications. (Jain et al. 2017) introduced a method which fuses appearance and motion for agnostic foreground object segmentation. Another application of flow augmentation is to provide temporal consistent semantic segmentation, which is explored by (Hur et al. 2016). Our network is conceptually closer to (Vertens et al. 2017), nevertheless we present a complete new design for the encoder and specially for the decoder. The proposed approach aims to use motion as a complementary cue to color. An overview of the proposed network is presented in Figure 10. To ob-

Table 16: Results on Cityscapes dataset. Our deep decoder when combined with both approaches provided substantial gains. In the case of deeplab v2 with DD we only had a lower score than our baseline for the bus class all the other classes we obtain better IoU scores, the only exception is motorcycle where we perform the same. For the comparison with deeplab v3+ our decoder provided a gain over the mean IoU and substantial gains for the class bus, truck and train, with 10, 11 and 6 percentage points respectively.

Method	Road	sidewalk	Building	Wall	Fence	Pole	Traffic light	Traffic Sign	Vegetation	Terrain	Sky	Person	Rider	Car	Truck	Bus	Train	Motorcycle	Bicycle	mIoU
DeepLab v2 (L. Chen et al. 2016)	96.	74.	89.	50.	42.	44.	49.	62.	90.	54.	92.	71.	49.	91.	65.	72.	45.	46.	66.	65.6
DeepLab v2 with DD	97.	79.	90.	52.	47.	53.	54.	67.	91.	62.	94.	75.	52.	93.	73.	70.	32.	46.	69.	68.1
DeepLab v3+ (L. Chen et al. 2018)	97.	77.	89.	50.	48.	47.	47.	61.	90.	59.	92.	71.	50.	92.	64.	65.	62.	46.	66.	67.1
DeepLab v3+ with DD	97.	77.	90.	51.	49.	52.	45.	63.	91.	56.	93.	71.	46.	93.	75.	77.	68.	47.	67.	68.7

Table 17: Runtime depending on the GPU DD-Net.

GPU	Forward Pass Time (ms)
GTX TITAN X	306
GTX 1080	272
GTX TITAN Xp	278
GTX 1080Ti	201
P100	210
GTX TITAN V	139

Table 18: Experiment optimizing DD-Net for runtime performance. Our full DD-Net can process 7 frames per second, while changing the encoder block can make DD-Net to process 14 frames per second. Further reducing the deep decoder to include only two decoder blocks makes our approach capable of processing 21 frames per second.

Setting	mIoU	Forward Pass Time (ms)
DD-Net	65.5	139
Inverted residual with DD	62.1	71
Inverted residual with slim DD	61.4	47

tain optical flow estimation for each image in the dataset, we used the FlowNet v2 model (Ilg et al. 2017) to predict the flow map between each image and its previous frame.

The flow augmentation takes two consecutive images and computes the flow. The flow representation used is the magnitude and direction in 2 channels. We choose early fusion as modality fusion technique based on the low computational impact. Late fusion with single encoder streams for RGB and flow are prohibited in terms of computational requirement and computation overhead. The input for the DD-Net segmentation is the RGB + magnitude and direction. The remaining network is our deep decoder network.

Our experiments will focus on the Cityscapes dataset. The dataset includes the previous image frame relative to each annotated image in a separate subset of video sequences, which we use to obtain optical flow predictions. We report results on the compressed version of cityscapes with 10 semantic classes. Table 19 presents the obtained re-

sults of DDNet and DDNet augmented with flow information. Some classes like sky, sign and pedestrians greatly benefit from the flow information, with sign and sky improving more than six percentage points, which is a strong gain for the already high quality segmentation obtained by DD-Net with RGB.

A qualitative comparison between our approach and its motion augmented version is presented in Figure 11. The columns are organized as follows, input image, groundtruth, DD-Net prediction and flow augmented DD-Net respectively. The first row is an example where the inclusion of motion can provide better segmentation for classes in which motion can be better capture, that is the case for the pedestrian class. The second row shows that even with an inferior mean IoU for the sidewalk class, in the flow augmented version, the specific instance presents superior segmentation values for this class when compared to the standard RGB DD-Net. The third row exemplifies the lower false positive detection rate from the augmented version of the network, the vegetation class suffers from inconsistent labelling in the center of the image for the RGB version of our technique. The last row presents an example where the flow augmented version of our approach is capable of better segment the poles, which is an extremely challenging class. The main outcome from the optical flow augmentation to our approach is that motion related classes, like pedestrians, can benefit from that. However for the specific case of the cityscapes dataset the gain is limited by the similar motion pattern of the forward moving car. We believe that datasets with richer motion patterns will further benefit from this strategy.

## 5 Conclusions

In this paper, we have proposed a new decoder that is composed by a set of shallow small networks for semantic segmentation. The new decoder consists of a new topology of skip connections, namely backward and stacked residual and with a novel weight function, in which we aim to re-balance

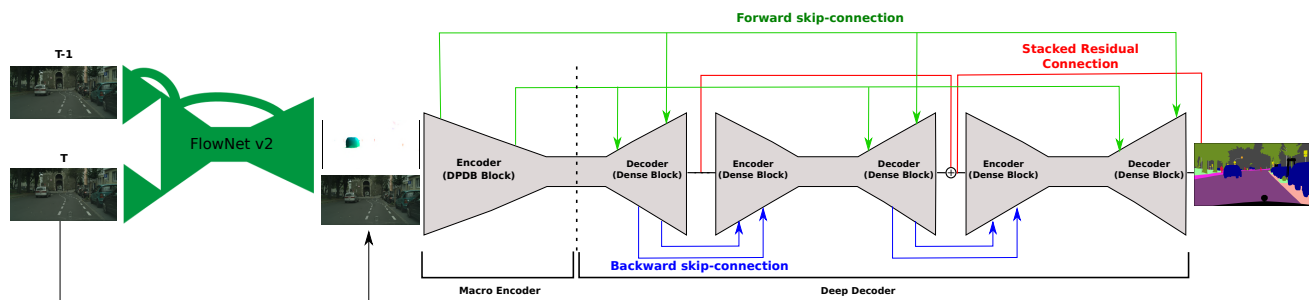


Fig. 10: DD-Net Architecture with flow augmentation. For visual simplification we do not show the full flow network, in our case FlowNet v2. To obtain optical flow estimation for each image in the dataset, we used the FlowNet v2 to predict the flow map between each image and its previous frame. After it the magnitude and direction are channel fused to the RGB image and given to our DDNet.

Table 19: Comparison between DDNet and DDNet augmented with flow on reduced version of the Cityscapes dataset. As seen the flow augmented version of DD-Net present superior results in the majority of the classes and an improvement in the mean IoU metric close to 1.5 percentage points.

Method	Sky	Building	Road	Sidewalk	Cyclist	Vegetation	Pole	car	Sign	Pedestrian	mIoU
DD-Net	85.27	88.99	<b>97.22</b>	<b>80.06</b>	<b>67.64</b>	90.32	<b>52.50</b>	91.08	60.94	68.95	78.30
DD-Net+FLow	<b>91.60</b>	<b>89.90</b>	97.15	79.63	66.03	<b>90.70</b>	52.13	<b>92.32</b>	<b>68.10</b>	<b>70.10</b>	<b>79.77</b>

classes to increase the attention of the networks to under represented objects. The ablation study shows that the design options effectively capture more information, are less conditioned to false positive detection and can produce a more efficient architecture for the given depth. Additionally, we show that a compact version of our approach is capable of iterative frame rate with minimum reduction of segmentation capabilities. Our experimental results show that our approach yields state-of-the-art results on the most relevant benchmarks for robotics and that motion clues can be used as extra input values to further improve segmentation.

**Acknowledgements** This work was partially funded by the Freiburg Graduate School of Robotics and a research project with Valeo Vision Systems, Ireland.

## References

- Amirul Islam, Md, Mrigank Rochan, Neil D. B. Bruce, and Yang Wang (2018). “Gated Feedback Refinement Network for Coarse-to-Fine Dense Semantic Image labeling”. In: *CoRR* abs/1806.11266. arXiv: [1806.11266](https://arxiv.org/abs/1806.11266). URL: <http://arxiv.org/abs/1806.11266>.
- Badrinarayanan, Vijay, Ankur Handa, and Roberto Cipolla (2015). “SegNet: A Deep Convolutional Encoder-Decoder Architecture for Robust Semantic Pixel-Wise Labelling”. In: *CoRR* abs/1511.00561. arXiv: [1511.00561](https://arxiv.org/abs/1511.00561). URL: <http://arxiv.org/abs/1511.00561>.
- Barron, Jonathan T and Ben Poole (2016). “The Fast Bilateral Solver”. In: *European Conference on Computer Vision (ECCV)*.
- Brostow, Gabriel J., Julien Fauqueur, and Roberto Cipolla (2008). “Semantic Object Classes in Video: A High-Definition Ground Truth Database”. In: *Pattern Recognition Letters*.
- Chen, Liang, George Papandreou, Iasonas Kokkinos, Kevin Murphy, and Alan Yuille (2016). “DeepLab: Semantic Image Segmentation with Deep Convolutional Nets, Atrous Convolution, and Fully Connected CRFs”. In: *CoRR* abs/1606.00915. arXiv: [1606.00915](https://arxiv.org/abs/1606.00915). URL: <http://arxiv.org/abs/1606.00915>.
- Chen, Liang, George Papandreou, Iasonas Kokkinos, Kevin Murphy, and Alan L Yuille (2015). “Semantic Image Segmentation with Deep Convolutional Nets and Fully Connected CRFs”. In: *International Conference on Learning Representations (ICLR)*.
- Chen, Liang, Yukun Zhu, George Papandreou, Florian Schroff, and Hartwig Adam (2018). “Encoder-Decoder with Atrous Separable Convolution for Semantic Image Segmentation”. In: *ECCV*, pp. 833–851.
- Chen, Yunpeng et al. (2017). “Dual Path Networks”. In: *CoRR* abs/1707.01629. arXiv: [1707.01629](https://arxiv.org/abs/1707.01629). URL: <http://arxiv.org/abs/1707.01629>.

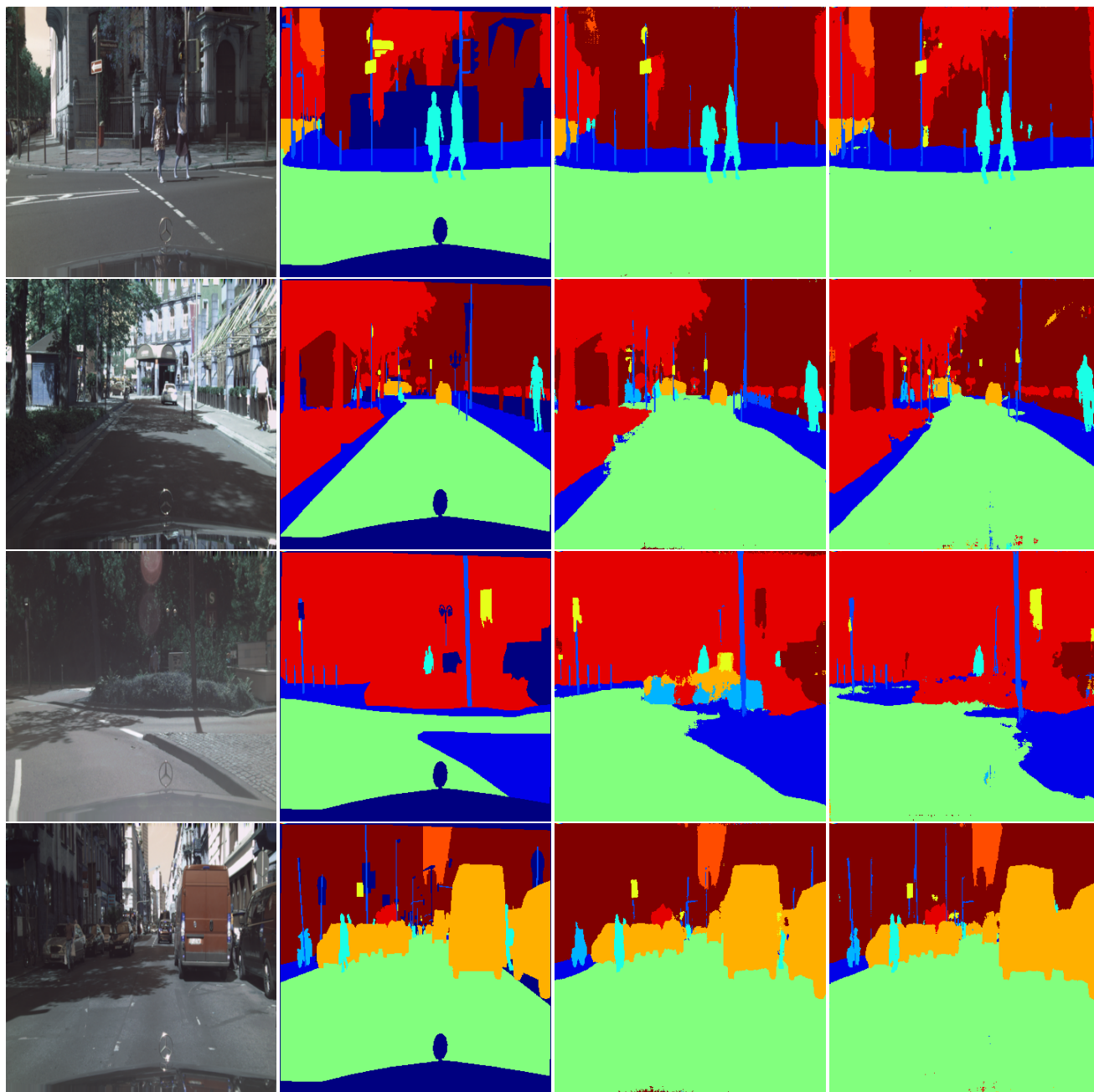


Fig. 11: Segmentation results between DD-Net and Flow augmented DD-Net. The first column shows input images, the second column the groundtruth, the third one the prediction from DD-Net without augmentation and the fourth column the DD-Net with flow augmentation. The first row is an example where the pedestrian class is better segmented by the flow augmented DD-Net. In the second row it can be seen that DD-Net alone presents less false positive detections for the building class but perform worst in the sidewalk segmentation. The third row is an inverse instance where DD-Net presents a considerable area in the center of the image with false positive detections of multiple classes, while the flow augmented version correctly segmentation that region as vegetation. The last row presents an example where the flow augmented version of our approach is capable of better segment the poles, which is an extremely challenging class.

Clevert, D., T. Unterthiner, and S. Hochreiter (2016). “Fast and accurate deep network learning by exponential linear units”. In: *International Conference on Learning Representations (ICLR)*.

Cordts, Marius et al. (2016). “The Cityscapes Dataset for Semantic Urban Scene Understanding”. In: *IEEE Conference on Computer Vision and Pattern Recognition (CVPR)*.

- Deng, J. et al. (2009). “ImageNet: A Large-Scale Hierarchical Image Database”. In: *IEEE Conference on Computer Vision and Pattern Recognition (CVPR)*.
- Eigen, David and Rob Fergus (2015). “Predicting Depth, Surface Normals and Semantic Labels with a Common Multi-scale Convolutional Architecture”. In: *International Conference on Computer Vision (ICCV)*, pp. 2650–2658.
- Fayyaz, Mohsen, Mohammad Hajizadeh Saffar, Mohammad Sabokrou, Mahmood Fathy, and Reinhard Klette (2016). “STFCN: Spatio-Temporal FCN for Semantic Video Segmentation”. In: *CoRR* abs/1608.05971. URL: <http://arxiv.org/abs/1608.05971>.
- Fu, Jun, Jing Liu, Yuhang Wang, and Hanqing Lu (2017). “Densely connected deconvolutional network for semantic segmentation”. In: *2017 IEEE International Conference on Image Processing (ICIP)*, pp. 3085–3089.
- Fu, Jun, Jing Liu, Yuhang Wang, and Hanqing Lu (2019). “Stacked Deconvolutional Network for Semantic Segmentation”. In: *IEEE Transactions on Image Processing*.
- Girshick, Ross (2015). “Fast R-CNN”. In: *Proceedings of the 2015 IEEE International Conference on Computer Vision (ICCV)*, pp. 1440–1448.
- H. Abdalnabi, Abrar, Stefan Winkler, and Gang Wang (2017). “Beyond Forward Shortcuts: Fully Convolutional Master-Slave Networks (MSNets) with Backward Skip Connections for Semantic Segmentation”. In: *CoRR* abs/1707.05537. arXiv: [1707.01629](https://arxiv.org/abs/1707.05537). URL: <http://arxiv.org/abs/1707.05537>.
- He, Kaiming, Xiangyu Zhang, Shaoqing Ren, and Jian Sun (2015). “Deep Residual learning for Image Recognition”. In: *CoRR* abs/1512.03385. arXiv: [1512.03385](https://arxiv.org/abs/1512.03385). URL: <http://arxiv.org/abs/1512.03385>.
- Huang, Gao, Zhuang Liu, Laurens van der Maaten, and Kilian Q Weinberger (2017). “Densely connected convolutional networks”. In: *IEEE Conference on Computer Vision and Pattern Recognition (CVPR)*.
- Hur, Junhwa and Stefan Roth (2016). “Joint Optical Flow and Temporally Consistent Semantic Segmentation”. In: *ECCV Workshops*.
- Ilg, E. et al. (2017). “FlowNet 2.0: Evolution of Optical Flow Estimation with Deep Networks”. In: *IEEE Conference on Computer Vision and Pattern Recognition (CVPR)*, pp. 1647–1655.
- Islam, Md. Amirul, Shujon Naha, Mrigank Roachan, Neil D. B. Bruce, and Yang Wang (2017). “Label Refinement Network for Coarse-to-Fine Semantic Segmentation”. In: *CoRR* abs/1703.00551. arXiv: [1703.00551](https://arxiv.org/abs/1703.00551). URL: <http://arxiv.org/abs/1703.00551>.
- Jain, Suyog, Bo Xiong, and Kristen Grauman (2017). “FusionSeg: Learning to combine motion and appearance for fully automatic segmentation of generic objects in videos”. In: *CVPR*.
- Jampani, Varun, Martin Kiefel, and Peter V. Gehler (2016). “Learning Sparse High Dimensional Filters: Image Filtering, Dense CRFs and Bilateral Neural Networks”. In: *IEEE Conference on Computer Vision and Pattern Recognition (CVPR)*.
- Jegou, Simon, Michal Drozdal, David Vazquez, Adriana Romero, and Yoshua Bengio (2016). “The One Hundred Layers Tiramisu: Fully Convolutional DenseNets for Semantic Segmentation”. In: *CoRR*. arXiv: [1611.09326](https://arxiv.org/abs/1611.09326). URL: <http://arxiv.org/abs/1611.09326>.
- Kendall, Alex, Vijay Badrinarayanan, and Roberto Cipolla (2015). “Bayesian SegNet: Model Uncertainty in Deep Convolutional Encoder-Decoder Architectures for Scene Understanding”. In: *CoRR*. arXiv: [1511.02680](https://arxiv.org/abs/1511.02680). URL: <http://arxiv.org/abs/1511.02680>.
- Kingma, D. and J. Ba (2014). “Adam: A method for stochastic optimization”. In: *CoRR*. arXiv: [1412.6980](https://arxiv.org/abs/1412.6980). URL: <http://arxiv.org/abs/1412.6980>.
- Kundu, Abhijit, Vibhav Vineet, and Vladlen Koltun (2016). “Feature Space Optimization for Semantic Video Segmentation”. In: *IEEE Conference on Computer Vision and Pattern Recognition (CVPR)*.
- Ladicky, Lubor, Christopher Russell, Pushmeet Kohli, and Philip H. S. Torr (2009). “Associative hierarchical CRFs for object class image segmentation.” In: *International Conference on Computer Vision (ICCV)*, pp. 739–746.
- Lazebnik, S., C. Schmid, and J. Ponce (2006). “Beyond Bags of Features: Spatial Pyramid Matching for Recognizing Natural Scene Categories”. In: *2006 IEEE Computer Society Conference on Computer Vision and Pattern Recognition (CVPR’06)*.
- Lin, G., C. Shen, A. van den Hengel, and I. Reid (2016). “Efficient piecewise training of deep structured models for semantic segmentation”. In: *IEEE Conference on Computer Vision and Pattern Recognition (CVPR)*.
- Lin, Tsung-Yi, Priya Goyal, Ross B. Girshick, Kaiming He, and Piotr Dollar (2017). “Focal Loss for Dense Object Detection”. In: *International Conference on Computer Vision (ICCV)*, pp. 2999–3007.
- Liu, Buyu and Xuming He (2015). “Multiclass Semantic Video Segmentation With Object-Level Active Inference”. In: *IEEE Conference on Computer Vision and Pattern Recognition (CVPR)*.
- Liu, Wei, Andrew Rabinovich, and Alexander Berg (2015). “ParseNet: Looking Wider to See Better”. In: *CoRR* abs/1506.04579. arXiv: [1506.04579](https://arxiv.org/abs/1506.04579). URL: <http://arxiv.org/abs/1506.04579>.
- Long, Jonathan, Evan Shelhamer, and Trevor Darrell (2015). “Fully Convolutional Networks for Semantic Segmentation”. In: *IEEE Conference on Computer Vision and Pattern Recognition (CVPR)*.

- Mostajabi, M., P. Yadollahpour, and G. Shakhnarovich (2015). “Feedforward semantic segmentation with zoom-out features”. In: *IEEE Conference on Computer Vision and Pattern Recognition (CVPR)*, pp. 3376–3385.
- Mousavian, Arsalan, Hamed Pirsiavash, and Jana Kosecka (2016). “Joint Semantic Segmentation and Depth Estimation with Deep Convolutional Networks”. In: *CoRR*. URL: <http://arxiv.org/abs/1604.07480>.
- Noh, Hyeonwoo, Seunghoon Hong, and Bohyung Han (2015). “Learning Deconvolution Network for Semantic Segmentation”. In: *International Conference on Computer Vision (ICCV)*, pp. 1520–1528.
- Oliveira, G., W. Burgard, and T. Brox (2016). “Efficient Deep Models for Monocular Road Segmentation”. In: *IEEE/RSJ International Conference on Intelligent Robots and Systems (IROS)*.
- Oliveira, G., W. Burgard, and T. Brox (2017). “Efficient and robust deep networks for semantic segmentation”. In: *The International Journal of Robotics Research*. DOI: [10.1177/0278364917710542](https://doi.org/10.1177/0278364917710542). URL: <http://dx.doi.org/10.1177/0278364917710542>.
- Oliveira, G., W. Burgard, and T. Brox (2018). “DPDB-Net: Exploiting Dense Connections for Convolutional Encoders”. In: *In Proc. of the IEEE Int. Conf. on Robotics and Automation (ICRA)*.
- Paszke, Adam, Abhishek Chaurasia, Sangpil Kim, and Eugenio Culurciello (2016). “ENet: A Deep Neural Network Architecture for Real-Time Semantic Segmentation”. In: *CoRR* abs/1606.02147. arXiv: [1606.02147](https://arxiv.org/abs/1606.02147). URL: <http://arxiv.org/abs/1606.02147>.
- Peng, Chao, Xiangyu Zhang, Gang Yu, Guiming Luo, and Jian Sun (2017). “Large Kernel Matters – Improve Semantic Segmentation by Global Convolutional Network”. In: *The IEEE Conference on Computer Vision and Pattern Recognition (CVPR)*.
- Raza, S. Hussain, Matthias Grundmann, and Irfan Essa (2013). “Geometric Context from Video”. In: *IEEE Conference on Computer Vision and Pattern Recognition (CVPR)*.
- Richter, Stephan R., Vibhav Vineet, Stefan Roth, and Vladlen Koltun (2016). “Playing for Data: Ground Truth from Computer Games”. In: *European Conference on Computer Vision (ECCV)*.
- Ronneberger, O., P.Fischer, and T. Brox (2015). “U-Net: Convolutional Networks for Biomedical Image Segmentation”. In: *Medical Image Computing and Computer-Assisted Intervention (MICCAI)*, pp. 234–241.
- Sandler, Mark, Andrew Howard, Menglong Zhu, Andrey Zhmoginov, and Liang-Chieh Chen (2018). “MobileNetV2: Inverted Residuals and Linear Bottlenecks”. In: *The IEEE Conference on Computer Vision and Pattern Recognition (CVPR)*.
- Simonyan, Karen and Andrew Zisserman (2015). “Very Deep Convolutional Networks for Large-Scale Image Recognition”. In: *International Conference on Learning Representations (ICLR)*.
- Tighe, Joseph and Svetlana Lazebnik (2010). “SuperParsing: Scalable Nonparametric Image Parsing with Superpixels”. In: *European Conference on Computer Vision (ECCV)*, pp. 352–365.
- Tran, Du, Lubomir D. Bourdev, Rob Fergus, Lorenzo Torresani, and Manohar Paluri (2016). “Deep End2End Voxel2Voxel Prediction”. In: *CVPR Workshop on Deep Learning in Computer Vision*.
- Valada, Abhinav, Gabriel Oliveira, Thomas Brox, and Wolfram Burgard (2017a). “Deep Multispectral Semantic Scene Understanding of Forested Environments Using Multimodal Fusion”. In: *2016 International Symposium on Experimental Robotics (ISER)*, pp. 465–477.
- Valada, Abhinav, Johan Vertens, Ankit Dhall, and Wolfram Burgard (2017b). “AdapNet: Adaptive Semantic Segmentation in Adverse Environmental Conditions”. In: *IEEE International Conference on Robotics and Automation (ICRA)*.
- Vertens, Johan, Abhinav Valada, and Wolfram Burgard (2017). “SMSnet: Semantic Motion Segmentation using Deep Convolutional Neural Networks”. In: *IEEE/RSJ International Conference on Intelligent Robots and Systems (IROS)*.
- Visin, Francesco et al. (2016). “ReSeg: A Recurrent Neural Network-Based Model for Semantic Segmentation”. In: *IEEE Conference on Computer Vision and Pattern Recognition (CVPR) Workshops*.
- Wang, Liwei, Chen-Yu Lee, Zhuowen Tu, and Svetlana Lazebnik (2015). “Training Deeper Convolutional Networks with Deep Supervision”. In: *CoRR* abs/1505.02496. arXiv: [1505.02496](https://arxiv.org/abs/1505.02496). URL: <http://arxiv.org/abs/1505.02496>.
- Wang, Yuhang et al. (2017). “Hierarchically Supervised Deconvolutional Network for Semantic Video Segmentation”. In: *Pattern Recognition*.
- Wojna, Zbigniew et al. (2017). “The devil is in the decoder”. In: *arXiv preprint arXiv:1707.05847*.
- Wu, Yan, Tao Yang, Junqiao Zhao, Linting Guan, and Jiqian Li (2017). “Fully Combined Convolutional Network with Soft Cost Function for Traffic Scene Parsing”. In: *International Conference on Intelligent Computing*.
- Yu, F. and V. Koltun (2016). “Multi-scale context aggregation by dilated convolutions”. In: *International Conference on Learning Representations (ICLR)*.
- Zhang, Zhenyu et al. (2018). “Joint Task-Recursive Learning for Semantic Segmentation and Depth Estimation”. In: *The European Conference on Computer Vision (ECCV)*.